

The crystal structure of a naturally occurring 5C pyrrhotite from Sudbury, its chemistry, and vacancy distribution

JOHAN P.R. DE VILLIERS,^{1,*} DAVID C. LILES,² AND MEGAN BECKER¹

¹Department of Materials Science and Metallurgical Engineering, University of Pretoria, Pretoria 0002, South Africa

²Department of Chemistry, University of Pretoria, Pretoria 0002, South Africa

ABSTRACT

The crystal structure of a naturally occurring pyrrhotite from the Copper Cliff North Mine, Sudbury, Canada, has been determined in the space group *Cmce* (formerly *Cmca*), and the positions and occupancy of the Fe and S atoms have been refined, together with their anisotropic atomic displacement parameters, to a conventional *R* value of 0.072. The summed occupancies of the Fe and Ni atoms [8.908 (Fe + Ni) per 10 S] are compared with the chemical composition, as determined by microprobe analysis, the latter giving a formula of $\text{Fe}_{8.892}\text{Ni}_{0.115}\text{S}_{10}$ or 9.007 (Fe + Ni) per 10 S.

The structure has cell dimensions of $a = 6.893(3)$ Å, $b = 11.939(3)$ Å, and $c = 28.63(1)$ Å. The S atoms are hexagonally close packed and adjacent Fe-S octahedra share faces that are perpendicular to the *c* direction. The Fe atoms in adjacent face-sharing octahedra also have the closest Fe-Fe interatomic distances. Some Fe atoms have partial occupancies, and together with the fully occupied sites, they add up to 71.26 (Fe + Ni) atoms per 80 S atoms in the unit cell, as compared with 72 atoms per 80 S atoms for Fe_9S_{10} .

The distribution of Fe in the partially occupied layers is different from that previously postulated for Fe_9S_{10} , with vacant sites present in two of the 10 layers. The partially occupied Fe sites are present in all the remaining cation layers, and there are therefore no cation layers containing completely filled atomic sites. Space group symmetry constrains the partially occupied cation sites to project on top of each other along the *c* axis, similar to the distribution of partially occupied sites in $\text{Fe}_{11}\text{S}_{12}$ (6C pyrrhotite).

Keywords: Pyrrhotite-5C, crystal structure, vacancy distribution, non-stoichiometry

INTRODUCTION

Pyrrhotite group minerals are important naturally occurring sulfides, and they are described as non-stoichiometric iron monosulfides having a general formula Fe_{1-x}S , with *x* ranging from 0 to 0.125. They are derivatives of the hexagonally close-packed NiAs structure, and the group consists of troilite (FeS) and pyrrhotites with continuously variable compositions that include Fe_7S_8 , Fe_9S_{10} , $\text{Fe}_{10}\text{S}_{11}$, and $\text{Fe}_{11}\text{S}_{12}$. Wang and Salveson (2005) give a recent review of the structures and properties of pyrrhotite. The structures of the pyrrhotites are complex and some are incommensurate, so that conventional structure analysis tools are not adequate to describe them. The modulated structure of $\text{Fe}_{10}\text{S}_{11}$ has been described by Yamamoto and Nakazawa (1982) using a four-dimensional description of the structure, with the fourth dimension describing the compositional and displacement modulations along the *c** direction. Izaola et al. (2007) revised this formulation, and a common model based on a centrosymmetric superspace group was proposed for the pyrrhotite family.

Morimoto et al. (1975) classified the pyrrhotites as either NA or NC types depending on the superstructures that develop as a result of the ordering of vacancies in the structures. In spite of numerous studies of pyrrhotites as a series of non-stoichiometric compounds, only two naturally occurring commensurate crystal

structures could be found in the literature. These are the structures of troilite, FeS (Evans 1970) and magnetic pyrrhotite, Fe_7S_8 (Tokonami et al. 1972). So, if Rietveld refinement of natural pyrrhotites or their quantification is envisaged, their crystal structures, with the exception of Fe_7S_8 , are not available, and refinement and quantification is thus not possible.

The so-called hexagonal pyrrhotite or non-magnetic pyrrhotite has been described from its Sudbury locality in Canada by Desborough and Carpenter (1965). Its symmetry and cell dimensions have been described as trigonal with cell dimensions $a = 6.893$ Å and $c = 28.635$ Å. Morimoto et al. (1975), in their review of the pyrrhotites, mention that the 5C structure is actually orthorhombic with space group (i.e., aspect symbol) *C*ca*, with cell dimensions $a = 6.885$ Å, $b = 11.944$ Å, and $c = 28.676$ Å.

Due to the renewed interest in the flotation properties of pyrrhotite, which is an important accessory sulfide in the production of nickel and platinum-group elements, its characterization and quantification are of importance. Traditionally, the pyrrhotites have been classified as either magnetic monoclinic pyrrhotite, or non-magnetic hexagonal pyrrhotite, and their distinction and quantification are required when interpreting their flotation behavior. Graham (1969) devised a method to determine the relative amounts of monoclinic and hexagonal pyrrhotite based on the relative intensities of the individual components of the split strongest powder X-ray diffraction peak. The development of more precise quantification of coexisting pyrrhotites using

* E-mail: johan.devilliers@up.ac.za

whole pattern refinement methods is dependent on the existence of refined crystal structure data. This is presented here for the non-magnetic 5C member of this important mineral group.

EXPERIMENTAL METHODS

Massive sulfide samples derived from the 100 ore body at Copper Cliff North mine in Sudbury, Canada, were provided by Vale INCO and pyrrhotite from them was selected for investigation. Numerous pyrrhotite grains were subsequently compositionally analyzed (Fig. 1) on a Jeol JXA 8100 Superprobe housed at the University of Cape Town, using an accelerating voltage of 25 kV and probe current of 20 nA. The compositional range of Copper Cliff North pyrrhotite as shown in Figure 1 illustrates that most compositions plot on the sulfur-rich side of the theoretical Fe_9S_{10} composition, with the maximum at 8.9 to 8.95 metal (Fe + Ni + Cu + Co) atoms per 10 S atoms. Also apparent is the continuous range in composition of these pyrrhotite specimens.

Numerous single crystals were examined, and only one suitable for single-crystal analysis was identified. After single-crystal data collection, the crystal was analyzed with a Cameca SX100 electron microprobe at the University of Pretoria, run at 20 kV accelerating voltage and 20 nA probe current. The average composition, based on 6 analyses and normalized to 10 S atoms, is given in Table 1. The average analysis for the crystal is 52.61 atom% S, 46.78 at% Fe, and 0.61 at% Ni. Initially, the structure analysis was attempted with a hexagonal cell and space group $P6_3/m$, but this was not successful. The unit-cell and diffraction data were then transformed to an orthorhombic setting based on the suggestion by Morimoto et al. (1975) that the symmetry is orthorhombic with space group C^{*ca} . Data were collected on a Bruker (Siemens) P4 diffractometer equipped with a Bruker SMART 1K CCD detector using graphite crystal monochromated $\text{MoK}\alpha$ radiation by means of a combination of phi and omega scans. Data reduction was performed using SAINT+ (Bruker 2001), and the intensities were corrected for absorption by multiple scans of symmetry equivalent reflections using SADABS (Bruker 2001). The intensities of 1264 unique reflections (sorted from 6041 reflections) were used in the refinements and the internal discrepancy factor of $R(\text{int}) = 0.032$ was obtained, which was considered to be acceptable. The crystal data are given in Table 1.

Structure determination was achieved using the SHELXD program (Sheldrick 1997) and refinement proceeded with 72 Fe atoms and 80 S atoms. Initially, because of the strong correlation between occupancy and atomic displacement parameters (ADP), an overall ADP for the Fe atoms was refined to establish the individual occupancy of the Fe atoms. Additional electron density was found at the position $(0,0,\frac{1}{2})$ and this was included in the refinement. The Fe sites that refined to occupancies close to 1.0 were then fixed at unity, and the individual isotropic ADPs were then allowed to vary, together with the occupancy of 3 Fe atoms. Neutral

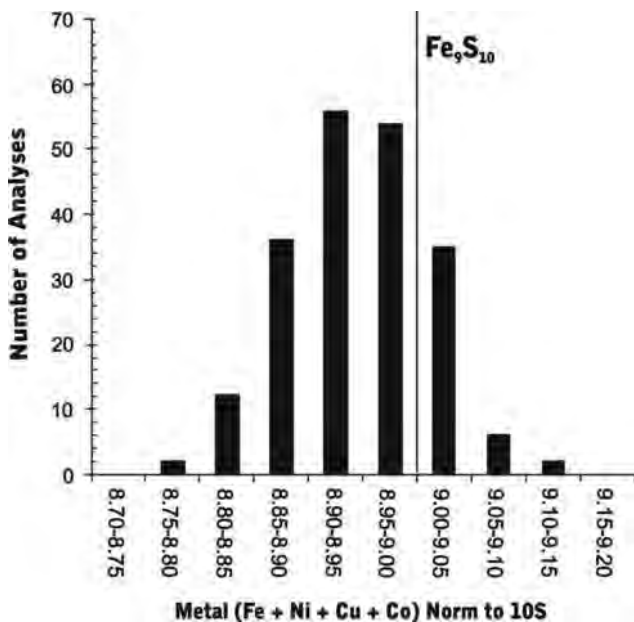


FIGURE 1. Distribution of 5C pyrrhotite compositions from the Copper Cliff North mine. The maximum in the distribution is in the range of 8.9 to 8.95 metal (Fe + Ni + Cu + Co) per 10 S.

scattering factors were used for all atoms. A small amount of Ni was allocated to the Fe1 site to account for its presence in the crystal. Lastly, the ADPs were refined anisotropically, together with the occupancies of the 3 Fe atoms. The refinement converged with a discrepancy factor $R_1 = 0.069$ for 915 observed reflections and $R_1 = 0.090$ for all 1264 measured reflections and 114 parameters. This included an extinction correction. After refinement, the goodness of fit parameter was $S = 1.331$. The largest residual electron density amounted to $1.13 \text{ e}/\text{\AA}^3$. Because of an unreasonably large ADP for the Fe atom at $(0,0,\frac{1}{2})$, it was then removed from the refinement. R_1 increased marginally to 0.0716 for 915 observed reflections and 0.0937 for 1264 measured reflections and 109 parameters. The goodness of fit parameter improved to 1.225. Residual electron density at position $(0,0,\frac{1}{2})$ after refinement was slightly higher at $1.53 \text{ e}/\text{\AA}^3$, but is still considered acceptable with the second highest density at $1.22 \text{ e}/\text{\AA}^3$. The ADPs of all atoms are now much more realistic and the very high ADP of the atom previously placed at $(0,0,\frac{1}{2})$ is of course eliminated. No further improvement in the refinement was achieved and the larger than normal R factor is thought to be a result of possible planar defects or stacking faults occurring in some layers in the structure. This was described by Posfai et al. (2000) using transmission electron microscopy. The composition, calculated from the refinement of the structure, is $\text{Fe}_{8.79}\text{Ni}_{0.118}\text{S}_{10}$.

The atomic positional and anisotropic displacement parameters are given in Tables 2 and 3, respectively, with the standard errors in parentheses. Table 4 gives the bond lengths, octahedral angular variance (OAV), and polyhedral quadratic

TABLE 1. Crystal data and structure refinement for 5C pyrrhotite

Identification code	pyrrhotite-5C
Empirical formula	$\text{Fe}_{8.79}\text{Ni}_{0.118}\text{S}_{10}$
Formula weight	6588.86
Temperature	293(2) K
Wavelength	0.71073 \AA
Crystal system, space group	Orthorhombic, $Cmce$ (formerly $Cmca$)
Unit-cell dimensions	$a = 6.893(3) \text{ \AA}$ $\alpha = 90^\circ$ $b = 11.939(3) \text{ \AA}$ $\beta = 90^\circ$ $c = 28.635(12) \text{ \AA}$ $\gamma = 90^\circ$
Volume	$2356.4(15) \text{ \AA}^3$
Z, Calculated density	8, 4.643 Mg/m^3
Absorption coefficient	12.516 mm^{-1}
F(000)	3154
Crystal size	$0.14 \times 0.06 \times 0.03 \text{ mm}^3$
θ range for data collection	$2.85\text{--}26.34^\circ$
Limiting indices	$-8 \leq h \leq 7, -8 \leq k \leq 14, -33 \leq l \leq 29$
Reflections collected/unique	6041/1264 [$R(\text{int}) = 0.0322$]
Completeness to $\theta = 25.00$	99.2%
Refinement method	Full-matrix least-squares on F^2
Data / restraints / parameters	1264 / 0 / 109
Goodness-of-fit on F^2	1.225
Final R indices [$I > 2\sigma(I)$]	$R_1 = 0.0716, wR_2 = 0.1513$
R indices (all data)	$R_1 = 0.0937, wR_2 = 0.1627$
Extinction coefficient	0.00003(2)
Largest diff. peak and hole	1.533 and $-2.125 \text{ e}/\text{\AA}^3$

TABLE 2. Positional parameters, occupancies, and equivalent isotropic atomic displacement parameters of the atoms in pyrrhotite-5C

Atom	x	y	z	Occ	U_{eq}
Fe1	0.5000	0.0	0.5000	0.76	0.019(1)
Ni1				0.24	0.019(1)
Fe2	0.2500	0.2500	0.5000	1.0	0.019(1)
Fe3	0.0	-0.0017(2)	0.6978(1)	1.0	0.018(1)
Fe4	0.5000	0.0140(2)	0.6007(1)	1.0	0.016(1)
Fe5	0.0	0.4855(2)	0.7008(1)	1.0	0.022(1)
Fe6	0.0	-0.0012(2)	0.5947(1)	0.857(10)	0.018(1)
Fe7	0.2732(2)	0.2395(1)	0.6015(1)	1.0	0.017(1)
Fe8	0.2311(3)	0.2569(2)	0.7015(1)	0.775(7)	0.018(1)
S1	0.5000	0.1683(3)	0.4466(1)	1.0	0.012(1)
S2	0.0	0.1650(3)	0.6483(1)	1.0	0.008(1)
S3	0.0	0.3326(3)	0.7531(1)	1.0	0.008(1)
S4	0.2500	0.0806(3)	0.7500	1.0	0.009(1)
S5	0.5000	0.1645(3)	0.6562(1)	1.0	0.008(1)
S6	0.5000	0.3301(3)	0.5496(1)	1.0	0.012(1)
S7	0.2515(4)	0.0828(2)	0.5484(1)	1.0	0.014(1)
S8	0.2499(4)	0.4154(2)	0.6477(1)	1.0	0.010(1)

Note: Standard errors are in parentheses and represent the last significant numbers.

elongation (PQE) as defined by Robinson et al. (1971) for the different octahedra surrounding the Fe atoms. These were calculated by the program XtalDraw (Downs and Hall-Wallace 2003).

Refinement in three subgroups was then attempted and tested using the Hamilton significance test (Hamilton 1965). Only these three were tested, as

TABLE 3. Anisotropic displacement parameters ($\text{\AA}^2 \times 10^3$) for pyrrhotite-5C

	U_{11}	U_{22}	U_{33}	U_{23}	U_{13}	U_{12}
Fe1	16(2)	36(2)	5(2)	-6(2)	0	0
Ni1						
Fe2	26(1)	19(1)	11(1)	-4(1)	-3(1)	-11(1)
Fe3	23(1)	20(1)	12(1)	5(1)	0	0
Fe4	30(1)	15(1)	3(1)	0(1)	0	0
Fe5	36(2)	16(1)	12(1)	6(1)	0	0
Fe6	35(2)	9(1)	9(1)	-5(1)	0	0
Fe7	10(1)	26(1)	15(1)	2(1)	0(1)	2(1)
Fe8	10(1)	25(1)	18(1)	-4(1)	-1(1)	6(1)
S1	12(2)	9(2)	16(2)	-5(2)	0	0
S2	6(2)	9(2)	9(2)	-1(1)	0	0
S3	5(2)	9(2)	11(2)	1(1)	0	0
S4	4(2)	11(2)	12(2)	0	-1(1)	0
S5	9(2)	9(2)	7(2)	-2(1)	0	0
S6	12(2)	8(2)	14(2)	-5(2)	0	0
S7	11(1)	10(1)	20(2)	2(1)	0(1)	1(1)
S8	6(1)	10(1)	16(1)	3(1)	1(1)	0(1)

Note: The anisotropic displacement factor exponent takes the form: $-2\pi^2 [h^2 a^{*2} U_{11} + \dots + 2 h k a^* b^* U_{12}]$.

TABLE 4. Metal-sulfur bond lengths (in angstroms) of the octahedra in 5C pyrrhotite

Atom	Bond	Lengths	Atom	Bond	Lengths	Atom	Bond	Lengths
Fe1	S1 ²	2.524(4)	Fe2	S1 ²	2.502(3)	Fe3	S2	2.442(4)
	S7 ⁴	2.415(3)		S6 ²	2.428(3)		S3	2.428(4)
	Fe4 ²	2.887(2)		S7 ²	2.430(3)		S4 ²	2.484(2)
				Fe7 ²	2.914(2)		S8 ²	2.452(3)
							Fe5	2.908(3)
							Fe6	2.953(4)
Avg. M-S		2.451			2.453			2.457
OAV		1.188			1.521			1.780
PQE		1.0012			1.0008			1.0006
Fe4	S1	2.562(5)	Fe5	S3	2.361(4)	Fe6	S2	2.510(5)
	S5	2.400(4)		S4 ²	2.499(3)		S6	2.393(5)
	S7 ²	2.419(3)		S5	2.488(4)		S7 ²	2.401(3)
	S8 ²	2.482(3)		S8 ²	2.446(3)		S8 ²	2.503(3)
	Fe1	2.887(2)		Fe3	2.908(3)		Fe3	2.953(4)
	Fe5	2.887(4)		Fe4	2.887(4)			
Avg. M-S		2.461			2.457			2.452
OAV		23.993			17.547			5.060
OQE		1.0072			1.0053			1.0019
Fe7	S1	2.580(3)	Fe8	S2	2.462(4)			
	S2	2.477(3)		S3	2.352(4)			
	S5	2.388(3)		S3	2.438(3)			
	S6	2.414(4)		S4	2.524(4)			
	S7	2.416(3)		S5	2.517(3)			
	S8	2.486(3)		S8	2.445(4)			
	Fe2	2.914(2)		Fe7	2.886(4)			
	Fe8	2.886(3)		Fe8	2.788(4)			
Avg. M-S		2.460			2.456			
OAV		24.874			19.898			
OQE		1.0076			1.0062			

Notes: The multiplicities of the bonds are given as superscripts, and the standard errors are in parentheses and represent the last significant numbers. The octahedral angular variance is in degrees squared and the polyhedral quadratic elongation is dimensionless. The shortest metal-metal distances are also given.

TABLE 5. Refinements of some subgroups of space group *Cmce*

Space group	R value	Dimension	Degrees of freedom	R-factor ratio	Hamilton test (0.5%)	Anisotropic ADP
<i>Cmce</i>	0.072	0	802			Pos. definite
<i>Cmc21</i>	0.061	98	1368	1.178	1.046	Non-pos def.
<i>C2cb</i>	0.059	69	1316	1.230	1.037	Non-pos def.
<i>Cm2a</i>	0.058	97	1204	1.248	1.052	Non-pos def.

Note: Although all refinements resulted in lower R values and significant improvements according to the Hamilton test (R -factor ratio > Test) at the 0.5% significance level, none resulted in reasonable atomic displacement parameters.

lower-symmetry subgroups would necessitate refinement of very large numbers of parameters. The results of the refinements of the subgroups are listed in Table 5.

Although significant improvements resulted, especially for space group *Cm2a*, none of the refinements resulted in reasonable atomic displacement parameters, and restraining these for some atoms using the ISOR command in SHELX also resulted in very distorted ellipsoids. The structure with space group *Cmce* is therefore considered to be the best candidate to describe the structure and vacancy distribution in 5C pyrrhotite.

It is also necessary to comment on the relatively high R factor of 0.072 and GOF of 1.225, and whether the structure described here is the correct one. If this structure is compared with the structure of monoclinic pyrrhotite described by Tokonami et al. (1974), the latter yielded an R of 0.093 for observed data and a goodness of fit of 1.69. Also, no anisotropic refinement was possible. Second, the overall structure of 5C pyrrhotite (positions of Fe and S atoms) is reasonable with realistic bond lengths and angles (Table 4). It is therefore quite compatible with the existing structure models of pyrrhotite. Third, refinement resulted in a calculated composition, which is reasonable for this structure type, and compares reasonably well with the microprobe analysis. The fact that partially occupied sites project directly above each other in 5C pyrrhotite was also observed by Koto et al. (1975) in their analysis of $\text{Fe}_{11}\text{S}_{12}$ and by Yamamoto and Nakazawa (1982) in their study of $\text{Fe}_{10}\text{S}_{11}$.

Finally, hand-sorted fragments of pyrrhotite were ground with a mortar and pestle, deposited on a low-background sample holder and examined with a PANalytical X'Pert PRO diffractometer equipped with an X'celerator detector and variable incident and diffracted beam slits. Refinement using *CoK α* was done using the commercial TOPAS software (Bruker 2005).

DESCRIPTION OF THE STRUCTURE

The structure is composed of hexagonally close-packed layers of S atoms octahedrally arranged around Fe atoms. These arrays form layers that are stacked perpendicular to the *c* axis. Figure 2 shows the atomic arrangement of the layer containing the vacant sites at $z = 0$.

The next layer of S and Fe atoms is arranged similarly to the first one, but with all Fe sites fully or partially filled (Fig. 3). The upper layer of S atoms in Figure 2 now comprises the lower layer of S atoms in the layer shown in Figure 3. The resultant stacking

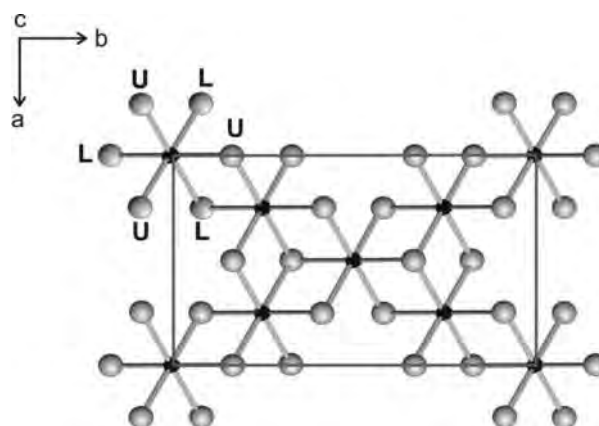


FIGURE 2. Octahedral arrangement of S atoms around the layer of Fe atoms at the origin of the unit cell ($z = 0$). The vacant cation sites are situated at the centers of the unit-cell edges. The lower layer of S atoms are labeled as L and the upper level as U.

arrangement comprises face-sharing octahedra stacked on top of each other. This face-sharing results in short Fe-Fe distances listed in Table 4, e.g., between Fe1 and Fe4, Fe4 and Fe5, etc.

The shortest Fe-Fe distances (2.886 Å) are between those atoms that project above each other, i.e., Fe4 and Fe5, Fe7 and Fe8. These are shorter than the values of 2.919, 2.947, and 2.984 Å, etc., given for troilite (Evans 1970). The face-shared arrangement of adjacent octahedra is shown in Figure 4, between the lower Fe7 and upper Fe8 octahedra.

The distribution of vacant and partially filled Fe sites in 5C pyrrhotite is shown in Figure 5, and this is compared with the distribution of vacant sites in monoclinic pyrrhotite, described by Tokonami et al. (1972). In this setting, the structure of the monoclinic pyrrhotite can be directly compared with that of 5C pyrrhotite. This choice of common unit cell facilitates comparison between the 5C and 4C pyrrhotites. This is also the cell of choice of Wang and Salveson (2005) in their review. It must be emphasized that the cell for monoclinic pyrrhotite shown in Figure 5 is not the true unit cell, but one formed by connecting the Fe atoms in the layers as shown.

The space group symmetry constrains the partially occupied sites (Fe6) to project on either side of the vacant sites (layers 0 and 5). The partially occupied sites with Fe8 in layers 2 and 3 as well in layers 7 and 8 project directly on top of each other. There seems to be a tendency for the partially filled sites to cluster together. This was also described by Koto et al. (1975) in their description of the vacancy arrangement of $\text{Fe}_{11}\text{S}_{12}$. In the latter case, two half-filled Fe sites project directly on top of each other. This was ascribed to the formation of a 1:1 intergrowth of defective (vacancy-containing) and filled layers. Such an intergrowth could not be constructed for the structure described here.

The occupancy of Fe in the different layers in the 5C pyrrhotite is shown in Figure 6a, compared to that of 4C pyrrhotite. A layer with all cation sites occupied by Fe atoms will have an occupancy of 1, and the occupancy of a layer with two vacant sites is 0.75. In 4C pyrrhotite, alternating layers contain either

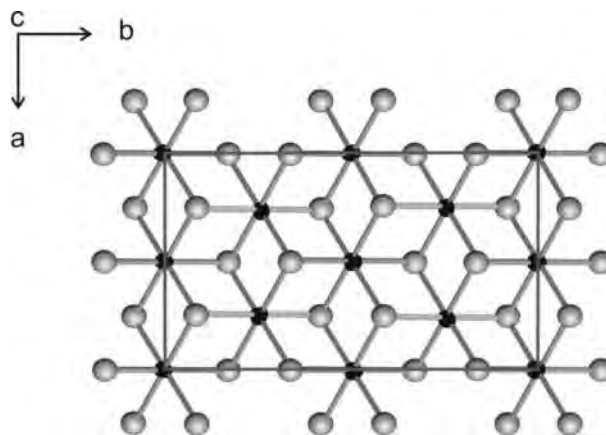


FIGURE 3. The atomic arrangement in the next layer of Fe and S atoms. The Fe8 atoms project directly on top of the almost vacant Fe9 sites, and they have an occupancy of 0.86.

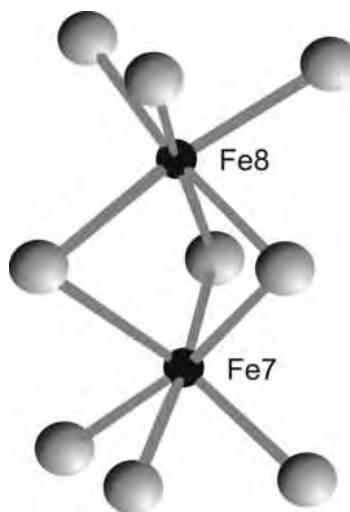


FIGURE 4. Adjacent face-sharing octahedra in 5C pyrrhotite, resulting in short Fe7-Fe8 distances.

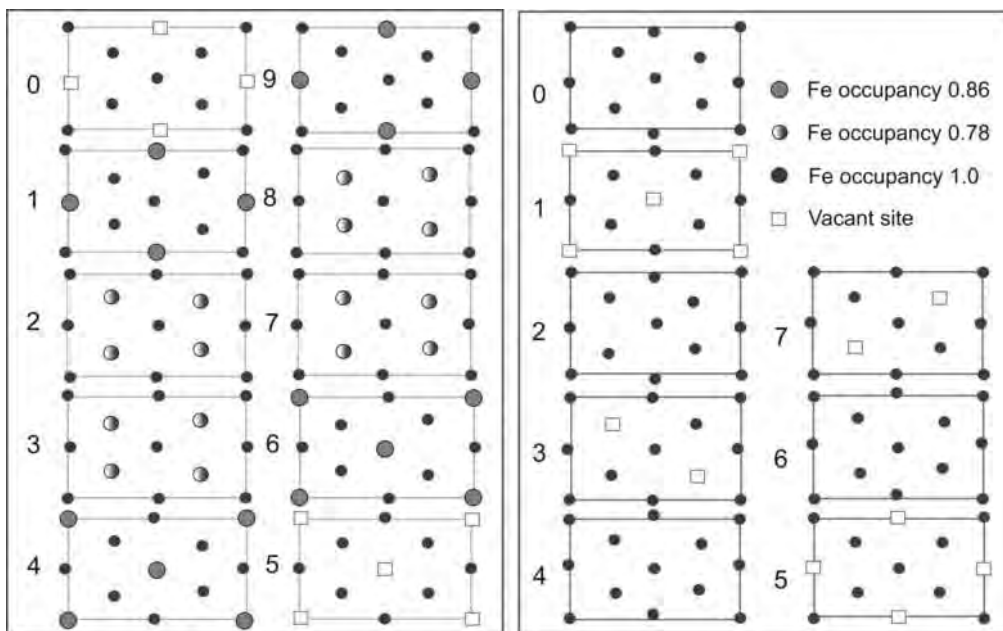


FIGURE 5. Distribution of vacant and partially occupied sites in 5C pyrrhotite (left diagram) as compared to the vacancy distribution in monoclinic pyrrhotite (right). The layers are labeled from 0 to 9 for 5C pyrrhotite and from 0 to 7 in 4C pyrrhotite. The sites with the partial occupancies are shown in different shades of gray. Layers 1, 3, 5, and 7 in 4C pyrrhotite are also described as the A, B, C, and D configurations.

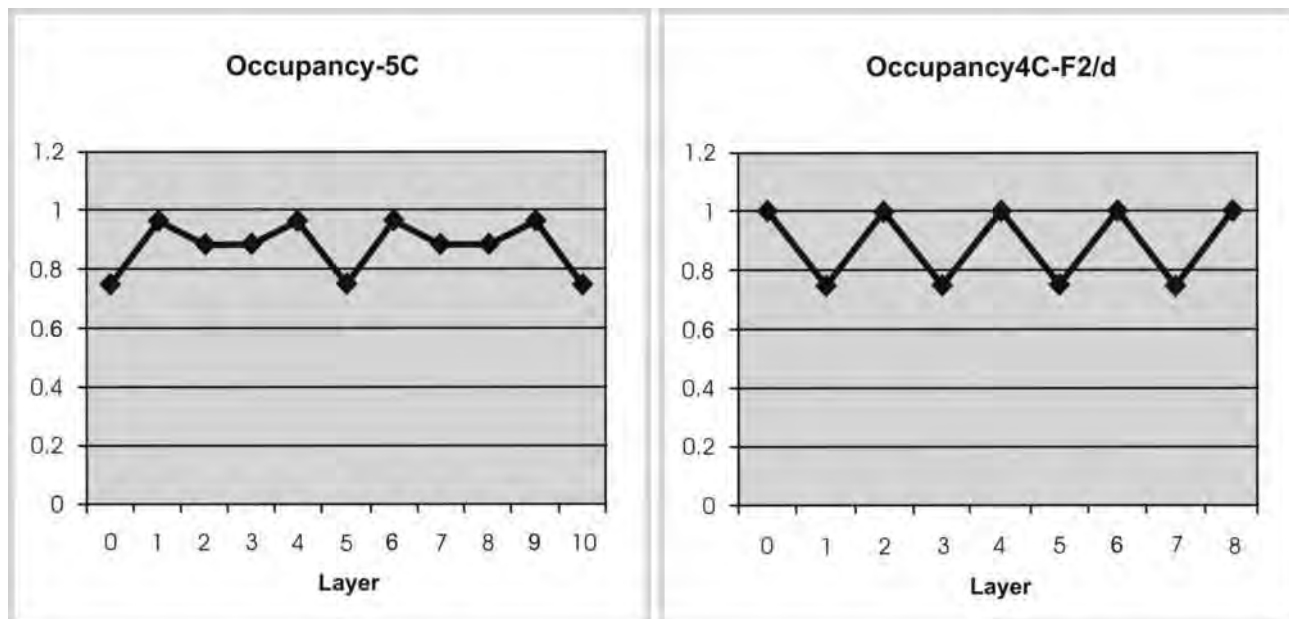


FIGURE 6. (a) Occupancy of Fe in the different layers of 5C pyrrhotite. The minimum occupancy of Fe is 0.75 in layers 0 and 5; the maximum is 0.968 in layers 1, 4, 6, and 9. The occupancy in layers 2, 3, 7, and 8 is 0.893. The average occupancy is 0.908. Layers 0 and 10 denote the borders of the unit cell. (b) Occupancy of Fe in monoclinic 4C pyrrhotite. This varies periodically between 1 and 0.75. Layers 0 and 8 denote the boundaries of the unit cell.

fully occupied layers or layers with 2 vacant sites out of a possible 8, giving the layer an occupancy of 0.75.

So, the occupancy of monoclinic pyrrhotite will show a sawtooth pattern with alternating maxima at 1 and minima at 0.75 as shown in Figure 6b. In 5C pyrrhotite, the occupancy in vacancy-containing layers 0 and 5 is 0.75; in layers 2, 3, 7, and 8, it is 0.893; and in layers 1, 4, 6, and 9, it is 0.968.

DISCUSSION

The structure of the 5C pyrrhotite has been discussed by various authors. Vaughan et al. (1971) described the mineral from the Strathcona mine, Sudbury, as hexagonal and postulated the structure as comprising single and double filled layers alternating with layers containing vacancies. Koto et al. (1975) in their analysis of the superstructure of a 6C pyrrhotite postulated an arrangement of filled and defect layers, where the occupancy of the Fe atoms in the defect layers is one half. This means that the structure is explained not by the ordering of filled and vacant Fe sites, but by the arrangement of adjacent partially occupied sites. Unfortunately, however, they do not give a full structure determination for 6C pyrrhotite with unit cell, space group, and atomic positions.

The structure described here consists of two layers containing vacancies and eight layers containing partial occupancies. This can be compared to the structure postulated by Yamamoto and Nakazawa (1982) using a superspace formulation. They describe the 5C structure as consisting of two layers with adjacent partially occupied sites alternating with three layers of adjacent partially occupied sites. This can be schematically described as AABBBCCDDD with the sites partially occupied. In the case of the 5C structure described here, the distribution could be described as AA'A(BD)CC'C(BD) where A' and C' are layers containing vacancies and (BD) are layers that contain partially

vacant sites in both the B and D configurations. The A, B, C, and D configurations correspond to the 1, 3, 5, and 7 layers in the 4C pyrrhotite in Figure 5. The structure therefore also consists of two layers alternating with three layers of partially occupied or vacant sites projecting above each other. The structure containing an additional partially occupied Fe site at $(0,0,\frac{1}{2})$ can therefore not be discounted entirely. This will have to be resolved if better crystals become available.

The non-stoichiometry most likely arises from the random stacking of layers containing vacancies with layers containing filled sites, giving rise to average structures with partially occupied sites. The partially occupied or vacant metal sites present in this structure can therefore be stacked in various proportions to give rise to a continuous variation in metal-to-sulfur ratios within the compositional limits of this structure type.

The superspace model of Yamamoto and Nakazawa (1982) was further refined by Izaola et al. (2007) who described the pyrrhotites in terms of the ordering of four different vacancy Fe layers and two different S layers. A new refinement of the incommensurate $\text{Fe}_{10}\text{S}_{11}$ (or $\text{Fe}_{0.91}\text{S}$) is presented by them. The use of this formulation to describe the partial occupancies of all pyrrhotites as a group is obviously desirable and needs to be investigated further.

The structural description given here can therefore be shown as giving the correct composition of the 5C structure type. The calculated powder XRD pattern is compared with that of monoclinic pyrrhotite in Figure 7. The single strongest peak of the 5C pyrrhotite is compared with that of the double peak of the 4C variety. This confirms the interpretation of Graham (1969).

A Rietveld refinement of hand-picked crystals of the copper CliffNorth material achieved excellent correspondence between observed and calculated intensities with a R_{wp} of 1.7% and a R_{Bragg} of 1.15% with a Goodness of Fit parameter of 1.41.

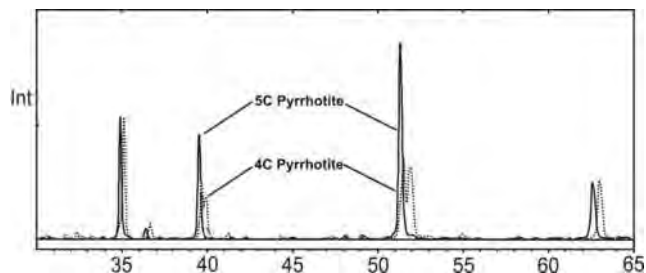


FIGURE 7. Calculated X-ray powder diffraction pattern showing the single peaks of the 5C pyrrhotite compared with the double peaks of monoclinic 4C pyrrhotite based on the structure of Tokonami et al. (1972).

The mechanism and reason for the non-stoichiometry is still a matter of dispute. A simple model that explains the magnetic properties of Fe_7S_8 requires the presence of Fe^{3+} in the vacancy layer. If four Fe^{2+} atoms are present on the fully occupied planes and one Fe^{2+} and two Fe^{3+} atoms on the planes containing vacancies, then the correct net magnetization of $2\mu_B$ is obtained. This model also explains the non-stoichiometry of the various pyrrhotites by a simple charge-balance mechanism, i.e., substitution of Fe^{3+} for Fe^{2+} , resulting in a deficiency of Fe to maintain electrical neutrality. The formula of Fe_7S_8 can therefore be written as $\text{Fe}_5^{2+}\text{Fe}_2^{3+}\text{S}_8$ and that for Fe_9S_{10} as $\text{Fe}_7^{2+}\text{Fe}_2^{3+}\text{S}_{10}$. The existence of both ferrous and ferric iron in monoclinic pyrrhotite was confirmed by Pratt et al. (1994) using X-ray photoelectron spectroscopy. On the other hand, no evidence of Fe^{3+} could be found by Mössbauer spectroscopy, (Oddou et al. 1992). Also, in a recent study by Letard et al. (2007) using X-ray magnetic dichroism, no evidence of ferric iron could be found in Fe_7S_8 pyrrhotite. If this is the case, then a more complicated mechanism is responsible for the non-stoichiometry, and for the stability of pyrrhotite relative to troilite. Clearly, this is an area that needs to be investigated.

ACKNOWLEDGMENTS

Microprobe analysis of the pyrrhotite single crystal by P. Gräser is gratefully acknowledged. Thanks also to Alison Tuling for help with the diagrams.

REFERENCES CITED

- Bruker (2001) SAINT+ Version 6.45, SADABS Version 2.10. BRUKER AXS Inc., Madison, Wisconsin.
 — (2005) DIFFRAC^{Plus} TOPAS Version 3. BRUKER AXS GmbH, Karlsruhe, Germany.
 Desborough, G.A. and Carpenter, R.H. (1965) Phase relations of pyrrhotite. *Economic Geology*, 60, 1431–1450.

- Downs, R.T. and Hall-Wallace, M. (2003) The American Mineralogist crystal structure database. *American Mineralogist*, 88, 247–250.
 Evans Jr., H.T. (1970) Lunar troilite: crystallography. *Science*, 167, 621–623.
 Graham, A.R. (1969) Quantitative determination of hexagonal and monoclinic pyrrhotites by X-ray diffraction. *Canadian Mineralogist*, 10, 4–24.
 Hamilton, W.C. (1965) Significance tests on the crystallographic *R* factor. *Acta Crystallographica*, 18, 502–510.
 Izaola, Z., González, S., Elcoro, L., Perez-Mato, J.M., Madariaga, G., and Garcia, A. (2007) Revision of pyrrhotite structures within a common superspace model. *Acta Crystallographica*, B63, 693–702.
 Koto, K., Morimoto, N., and Gyobu, A. (1975) The superstructure of the intermediate pyrrhotite. I. Partially disordered distribution of metal vacancy in the 6C type, $\text{Fe}_{11}\text{S}_{12}$. *Acta Crystallographica*, B31, 2759–2764.
 Letard, I., Saintavrit, P., and Deudon, C. (2007) XMCD at $\text{Fe L}_{2,3}$ edges, Fe and S K edges on Fe_7S_8 . *Physics and Chemistry of Minerals*, 34, 113–120.
 Morimoto, N., Gyobu, A., Mukaiyama, H., and Izawa, E. (1975) Crystallography and stability of pyrrhotites. *Economic Geology*, 70, 824–833.
 Oddou, J.L., Jeandey, C., Mattei, J.L., and Fillion, G. (1992) Mössbauer study of the low-temperature transition in pyrrhotite. *Journal of Magnetism and Magnetic Materials*, 104–107, 1987–1988.
 Posfai, M., Sharp, T.G., and Konty, A. (2000) Pyrrhotite varieties from the 9.1 km deep borehole of the KTB project. *American Mineralogist*, 85, 106–1415.
 Pratt, A.R., Muir, I.J., and Nesbitt, H.W. (1994) X-ray photoelectron and Auger electron spectroscopic studies of pyrrhotite and mechanism of air oxidation. *Geochimica et Cosmochimica Acta*, 58, 827–841.
 Robinson, K., Gibbs, G.V., and Ribbe, P.H. (1971) Quadratic elongation: A quantitative measure of distortion in coordination polyhedra. *Science*, 172, 567–570.
 Sheldrick, G.M. (1997) SHELX97—Programs for crystal structure analysis (Release 97-2). Institut für Anorganische Chemie der Universität, Göttingen, Germany.
 Tokonami, M., Nishiguchi, K., and Morimoto, N. (1972) Crystal structure of a monoclinic pyrrhotite (Fe_7S_8). *American Mineralogist*, 57, 1066–1080.
 Vaughan, D.J., Schwarz, E.J., and Owens, D.R. (1971) Pyrrhotites from the Strathcona Mine, Sudbury, Canada: A thermogravimetric and mineralogical study. *Economic Geology*, 66, 1131–1144.
 Wang, H. and Salveson, I. (2005) A review on the mineral chemistry of the non-stoichiometric iron sulphide, Fe_{1-x}S ($0 \leq x \leq 0.125$): polymorphs, phase relations and transitions, electronic and magnetic structures. *Phase Transitions*, 78, 547–567.
 Yamamoto, A. and Nakazawa, H. (1982) Modulated structure of the NC-type ($N = 5.5$) pyrrhotite, Fe_{1-x}S . *Acta Crystallographica*, A38, 79–86.

MANUSCRIPT RECEIVED AUGUST 27, 2008

MANUSCRIPT ACCEPTED MAY 13, 2009

MANUSCRIPT HANDLED BY LAURENCE GARVIE

NOTE ADDED IN PROOF

Subsequent to the submission of this paper, a second suitable crystal was found, and its X-ray data refined. The resultant *R*-factor was $R = 0.06$, and the unit-cell and structure parameters were very similar to the values given here. These are available from the author on request.